


ELECTROPHYSIOLOGY

Localization and Spread of Challenging Conduction Gaps of Pulmonary Veins for Atrial Fibrillation Cryoablation

Keita Miki  | Koji Fukuda | Michinori Hirano | Koichi Sato | Shohei Ikeda | Mariko Shinozaki | Morihiko Takeda

Department of Cardiology, International University of Health and Welfare Hospital, Tochigi, Japan

Correspondence: Koji Fukuda (fukuda-k@iuhw.ac.jp)

Received: 11 March 2024 | **Revised:** 10 November 2024 | **Accepted:** 8 December 2024

Funding: The authors received no specific funding for this work.

Keywords: atrial fibrillation | cryoablation | cryoballoon | high-resolution mapping | pulmonary vein isolation | resistant conduction gap

ABSTRACT

Background: Cryoballoon ablation has been widely performed in patients with paroxysmal atrial fibrillation (AF). In some challenging pulmonary veins (PVs), the procedure requires additional touch-up applications against the residual conduction gaps. It implies that there could exist difficult sites to cover with standard cryoballoon applications (CBAs), resulting in resistant conduction gaps (RCGs). This study aims to characterize the RCGs after initial CBAs.

Methods: We retrospectively enrolled 90 consecutive paroxysmal AF patients in our institute from January 2018 to December 2021 (66.5 ± 8.9 [SD] year-old, male/female 58/32). The RCGs after initial CBAs were mapped and analyzed with a high-resolution mapping (HRM) catheter. The PVs isolated using HRM were classified as HRM group. The PVs isolated without HRM, if isolated with a total of one or two CBAs, were classified as Control group.

Results: Whereas 325 PVs were isolated without HRM, 29 PVs had RCGs which were mapped and identified with HRM (HRM group): 15 right inferior pulmonary veins (RIPVs), 11 left superior PVs (LSPVs), and 3 left inferior PVs (LIPVs). In HRM group, the rate of broad RCGs in each PV extending over 2 or 3 segments of PV was almost double that of one-segment RCGs. The width of RCGs significantly correlated with nadir balloon temperature ($R = 0.42$; $p = 0.021$) and iTT_{15} ($R = -0.44$; $p = 0.015$).

Conclusions: After standard CBAs, most RCGs were demonstrated to spread from the bottom to the posterior wall of RIPV and from the roof to the anterior wall of LSPV. The width of the RCGs was found to be correlated with parameters of balloon temperature, such as T_{nadir} and iTT_{15} .

1 | Introduction

Pulmonary vein (PV) isolation using a second-generation cryoballoon (CB) catheter (Arctic Front Advance; Medtronic, Minneapolis, MN, USA) has become a widespread procedure for the treatment of patients with atrial fibrillation (AF) [1, 2]. The CB, which is designed to achieve unique cooling across the entire distal hemisphere of the balloon, has been demonstrated to be highly effective in accomplishing freedom from AF [3]. However, there are several challenging cases to achieve durable PV isolation

even by multiple cryoballoon applications (CBAs), and touch-up radiofrequency (RF) applications are necessary at a certain rate [4]. It implies that there could exist difficult sites to cover with standard CBA, resulting in resistant conduction gaps (RCGs). However, the detailed distribution and spread of RCGs are not fully investigated, even though these data are indispensable for efficient and effective PV isolation with CB. Furthermore, biophysical predictors associated with the RCGs remain to be examined, whereas balloon temperature or time to isolate PVs have been reported to be makers of durable PV isolation [5, 6].

This study aimed to elucidate the characteristics of the RCGs as follows: (1) the distribution and width of RCGs after standard CBAs using high-resolution mapping (HRM); (2) the relationship between balloon temperature and the width of RCGs.

2 | Methods

2.1 | Study Design and Population

We retrospectively enrolled 90 consecutive patients who underwent their first paroxysmal AF cryoablation in our hospital from January 2018 to December 2021. The patient inclusion criteria for enrollment were as follows: (1) a diagnosis of paroxysmal AF in accordance with the 2014 American Heart Association/American College of Cardiology/Heart Rhythm Society guidelines on the management of patients with paroxysmal AF [1], (2) treatment with cryoablation for paroxysmal AF, and (3) age from 20 to 85 years. Patients who had a left common PV, confluent inferior PV, extremely large antrum in a cardiac computed tomography (CT) scan before the procedure, and any contraindication to the procedure were excluded. The present study was approved by the International University Health and Welfare Institutional Review Board (No.13-B-293).

2.2 | Procedure Setups

All antiarrhythmic drugs were discontinued for at least five half-lives before the procedure. A cardiac CT scan of the left atrium (LA) was performed to examine the PV anatomy. Procedures were performed under deep sedation. Intravenous heparin was administered in a dose of 3000–4000 IU after the insertion of the sheaths into the subclavian and femoral veins. An activated clotting time >300 s was maintained during the procedure in LA using continuous infusion of heparin following an initial bolus (5000 IU) after the insertion of the sheaths to the LA. Standard multielectrode catheters were positioned in the coronary sinus (CS) and right ventricular apex. Two long sheaths (Daig SLO; Abbott, St. Paul, MN, USA) were introduced into the LA using a single atrial transseptal puncture technique under intracardiac echography guidance. Contrast cardiac angiography of the LA was performed through the two long sheaths placed in the left and right superior PVs during rapid ventricular pacing at 200 beats per minute to confirm the anatomy of bilateral PVs. One of the two long sheaths was exchanged into a 15-F steerable sheath (FlexCath; Medtronic, Minneapolis, MN, USA) for a cryoballoon.

2.3 | Ablation Procedures

All patients underwent PV isolation using a 28-mm CB (Arctic Front Advance) over a 20-mm circular inner lumen mapping catheter (Achieve; Medtronic, Minneapolis, MN, USA). The 3 right superior PVs (RSPVs) of 3 patients were treated with RF energy from the beginning because of anatomical issues, such as the atypical PV branch near the RSPV by the operator's decision and the other PVs (RIPV, LSPV and LIPV) were applied with cryoenergy. The 3 RPVs (both RSPV and RIPV) of the 3 patients were excluded from the analyses. The CB was once inflated on the distal side of a PV and its complete occlusion was confirmed

with a contrast medium, followed by being pulled back until the contrast medium leaked into the LA. After that, the balloon was gently advanced, aiming for optimal balloon-to-PV ostium contact. The quality of PV occlusion was graded from 1 to 4 as mild, medium, subtotal, or total. After verification of the complete sealing of the PV, a freeze cycle of 3 min was applied. Freeze applications were early stopped and the balloon was repositioned when the CB temperature fell below -60°C or the esophageal temperature went down below 15°C . During cryoablation of the right PVs, high-output right phrenic nerve stimulation (20–25 mA, 1000–1200 ms) was performed using a diagnostic catheter placed in the subclavian vein. Cryoablation was immediately stopped whenever the diminished diaphragmatic motion or the attenuation of diaphragmatic compound motor action potential amplitude was observed. CBAs were interrupted if neither PV isolation nor -35°C within 120 s was achieved. To analyze the CBAs that were sufficient to create durable lesions, CBAs with less than 120 s were not counted in the number of applications. Each PV isolation was confirmed by a bidirectional conduction block using a circular mapping catheter (Libero; Japan Lifeline, Tokyo, Japan). During freeze applications, the time to PV isolation was evaluated. If PV isolation was not accomplished after the 1st or 2nd CBA, then HRM was performed to identify RCGs at the discretion of the operator. In the second CBA, residual conduction gaps, especially detected by HRM, were treated with directing a CB at the RCGs, rather than simply aiming for the complete occlusion of the target PV. The PVs isolated using HRM were classified as HRM group. The PVs isolated without HRM, if isolated with a total of one or two CBAs, were classified as Control group.

2.4 | High-Resolution Electroanatomic Maps

The HRM of PVs was performed by using PentaRay catheter (Biosense Webster, Diamond Bar, CA, USA) and 3D Navigation System (CARTO3; Biosense Webster, Diamond Bar, CA, USA) with CONFIDENSE TM Module. The PentaRay catheter has five soft and flexible spines. Each spine has four electrodes with 2–6–2 mm interelectrode spacing, resulting in 10-bipolar mapping available. During the LA mapping, 5 ms local activation time (LAT) stability, 3 mm catheter stability, and 1 mm density were set as a filter of the continuous mapping. Using this catheter setup, the endocardial surface of left PVs was mapped at a cycle length of 500 ms from CS distal pacing to separate the left atrial appendage and PV electrogram, while right PVs were done under the sinus rhythm. We were especially cautious when manipulating the multielectrode catheter at the PV-LA junction to acquire the mapping points from the entire circumferential wall. The criteria used for beat acceptance included a stable cycle length, respiratory gating, stable catheter location, and stable catheter signal compared to adjacent points. The mapping window was automatically set by the system. The system annotated the largest bipolar electrogram within the mapping window. The Ripple Mapping, one of the functions of the CONFIDENSE TM Module, enables us to visualize the movement of all bipolar electrograms. Bars show the local voltage of the bipolar electrogram on the surface of the anatomical chamber. With multiple points, these can visualize the movement of electrograms like a ripple. It allows us to evaluate the propagation of all bipolar electrograms.

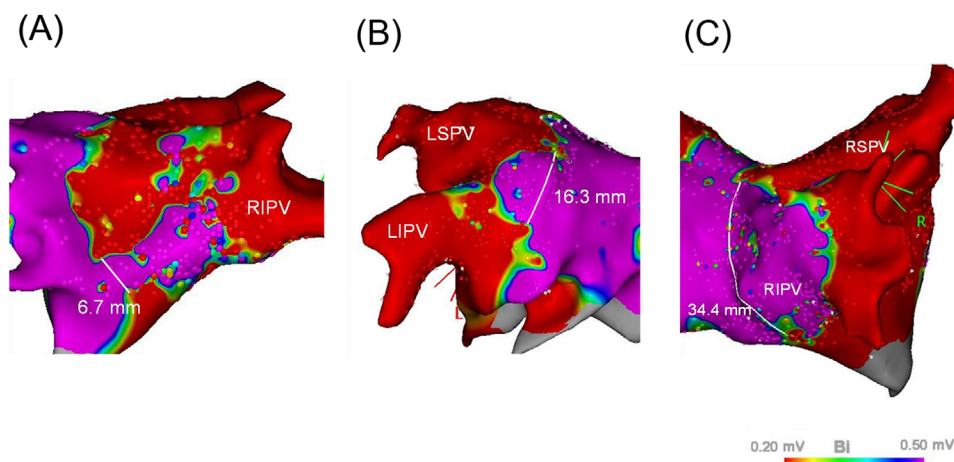


FIGURE 1 | Representative cases of RCGs identified in voltage map by using HRM. The voltage map was obtained during coronary sinus pacing. Each RCG was classified into the division of the antrum of each PV. (A) A one-segment RCG (6.7 mm) was identified on the bottom of RIPV. (B) A two-segment RCG (16.3 mm) was identified on the posterior wall to the carina of LIPV. (C) A three-segment RCG (34.4 mm) was identified on the bottom, posterior wall, and carina of RIPV. HRM, high-resolution mapping; LIPV, left inferior pulmonary vein; PV, pulmonary vein; RCG, resistant conduction gap; RIPV, right inferior pulmonary vein. [Color figure can be viewed at [wileyonlinelibrary.com](https://onlinelibrary.wiley.com)]]

2.5 | Evaluation of RCGs

On HRM, we set the bipolar voltage threshold for the voltage map at 0.20–1.0 mV. The voltage thresholds of <0.2, 0.2–0.5, and >0.5 mV were classified into dense scar, damaged viable tissue, and healthy tissue, respectively. The present study aims to evaluate the remaining voltage area in the vicinity of pulmonary vein, which might lead to AF recurrence, including not only the ablation area by CBA but also the antrum after standard CBAs by using HRM. Therefore, the geometrical RCG was defined as the remaining voltage area (more than or equal to 0.2 mV) between dense scars on the supposed extensive encircling PV isolation line where the outlines of the upper and lower PV isolation areas were connected with a line and assumed to be one large circle. The width of the gaps was measured as the remaining voltage region on the supposed line (Figure 1). The present study aims to evaluate the remaining voltage area in the vicinity of PV, which might lead to the recurrence, including the antrum in the challenging PVs to isolate by standard CBAs. The geometrical RCG was defined as the remaining voltage area (more than or equal to 0.2 mV) between dense scars on the supposed extensive encircling PV isolation line where the outlines of the upper and lower PV isolation areas were connected with a line. The surrounding area of each PV was divided into five sites to evaluate RCGs: anterior and posterior wall of PV, anterior and posterior carina, roof in the superior PV, and bottom in the inferior PV. Figure 1A–C indicates representative cases of 1-segment, 2-segment, and 3-segment RCGs, respectively. RSPV was excluded from the analyses because none of the patients needed to use HRM.

2.6 | Biophysical Data

The cryoablation binary data files stored in the CryoConsole were used to analyze various biophysical measurements, including (1) T_{slow} representing the temperature at the starting point of the slow cooling phase (the earliest time point at which the temperature

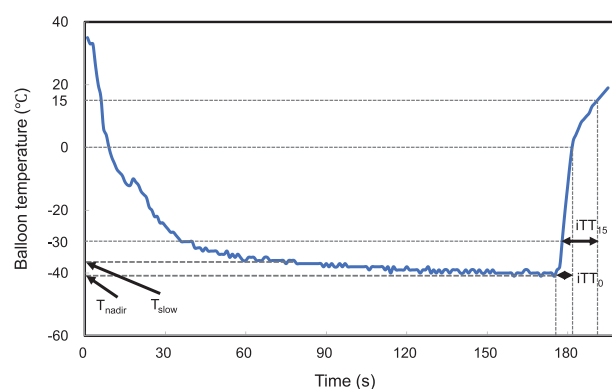


FIGURE 2 | Typical cryoballoon temperature–time curve during a single 3-min freeze. iTT_0 , the time from freeze termination until 0°C; iTT_{15} , the time from -30°C to 15°C ; T_{nadir} , the lowest temperature attained during a given cryoballoon application; T_{slow} , the temperature at the starting point of the slow cooling phase (the earliest time point at which the temperature change was $<1^{\circ}\text{C/s}$ averaged over 3 s). [Color figure can be viewed at [wileyonlinelibrary.com](https://onlinelibrary.wiley.com)]]

change was $<1^{\circ}\text{C/s}$ averaged over 3 s), (2) T_{nadir} representing the lowest temperature attained during a given CBA, (3) iTT_0 representing the time from freeze termination until 0°C, and (4) iTT_{15} representing the time from -30 to 15°C (Figure 2). To avoid any confounding effects of repeated CBAs, only the first CBA at each PV was analyzed.

2.7 | Study Follow-Up

Regular follow-up intervals consisted of outpatient clinic visits at 1, 3, 6, and 12 months after the procedure and included a detailed history for arrhythmia-related symptoms (palpitations, chest discomfort, fatigue, and dizziness), 12-lead electrocardiogram, and 24-h ambulatory ECG monitoring.

TABLE 1 | Clinical characteristics of study patients ($n = 90$).

General characteristics	
Age (year)	66.5 ± 8.9
Male sex, n (%)	58 (64.4)
Body surface area (m^2)	1.65 ± 0.21
Body mass index (kg/m^2)	24.2 ± 4.7
eGFR ($\text{mL}/\text{min}/\text{m}^2$)	77.4 ± 12.1
BNP (pg/mL)	47.9 ± 39.9
Diabetes mellitus, n (%)	12 (13.3)
Hypertension, n (%)	47 (52.2)
CHADS ₂ score	0.9 ± 0.9
CHA ₂ DS ₂ -VASc score	1.8 ± 1.3
Medication, n (%)	
Na channel blocker	31 (34.4)
β -blocker	37 (41.1)
Ca channel blocker	6 (6.6)
Warfarin	0 (0)
DOAC	90 (100)
Echocardiographic parameters	
LVEF (%)	66.1 ± 8.8
LAD (mm)	37.6 ± 5.8
LAVI (cm^3/m^2)	36.2 ± 14.0

Abbreviations: AF, atrial fibrillation; BNP, B-type natriuretic peptide; DOAC, direct oral anticoagulant; eGFR, estimated glomerular filtration rate; LAD, left atrial diameter; LAVI, left atrial volume index; LVEF, left ventricular ejection fraction.

2.8 | Statistical Analysis

Continuous data following normal distribution were expressed as mean \pm standard deviation (SD) and were compared using Student's t test or one-way analysis of variance (ANOVA). Categorical data were expressed as counts (percentage) and were compared using a chi-square test or Fisher's exact test if needed. Associations between continuous variables were assessed using Spearman's rank correlation tests. p values less than 0.05 were considered to be statistically significant. Analyses were performed by using JMP 12 (SAS Institute Inc., Cary, NC, USA).

3 | Results

3.1 | Clinical Characteristics and Cryoablation Results

The clinical patient characteristics are summarized in Table 1. The mean age was 66.5 ± 8.9 [SD] years (male/female 58/32). The mean CHADS₂ and CHA₂DS₂-VASc scores of this population were not high and most patients had a preserved ejection fraction. The left atrial volume index (LAVI) was mildly dilated.

The flowchart of CBAs is shown in Figure 3. Three patients underwent RSPV isolation with RF energy from the beginning

because of anatomical issues, such as the atypical PV branch near the RSPV by the operator's decision. The other PVs (right inferior PV [RIPV], left superior PV [LSPV], and left inferior PV [LIPV]) were applied with cryoenergy first. Therefore, the right PV data in the three patients were excluded from the analyses. As a result, the remaining 354 PVs were analyzed. Twenty-nine PVs, in which RCGs were detected with HRM, were defined as HRM group: 15 RIPVs, 11 LSPVs, and 3 LIPVs. The remaining 325 PVs were isolated by cryoablation without HRM (one CBA in 269 PVs, two CBAs in 48 PVs, and three CBAs in 8 PVs). The 317 PVs isolated with one or two CBAs without HRM were analyzed as Control group.

3.2 | Gap Identification With High-Resolution Mapping

Figure 4 shows the distribution of RCGs in the 29 PVs in HRM group (15 RIPVs, 11 LSPVs, and 3 LIPVs). The total RCGs in RIPV, LSPV, and LIPV were 28, 20, and 5, respectively. Figure 5A shows the spread of RCGs. RIPVs often had broad RCGs with multiple segments that extended from the bottom to the posteroinferior segments. Concerning LSPV, broad RCGs were often detected from the anterior wall to the roof. Figure 5B represents the distribution of the number of gap segments and the average width of the RCGs. The rate of broad RCGs extending over multiple segments (two or three) in each PV was almost double that of 1-segment RCGs.

3.3 | Procedural Outcomes

Twenty-nine PVs in HRM group were isolated by cryoablation ($N = 24$) or touch-up RF ablation ($N = 5$). The procedural data and biophysical data in each PV are shown in Table 2. Compared with Control group, HRM group significantly had lower occlusion grade, lower T_{slow} , T_{nadir} , and shorter $i\text{TT}_0$, $i\text{TT}_{15}$ in RIPV and LSPV. Most of the interrupted applications were less than or around 60 s, which we thought was insufficient to achieve PV isolation. No additional CBAs were performed after completing PV isolation with HRM. In Control group, patients who needed additional reconnection procedures were treated with CBA or touch-up RFCA while referring to the electrical potentials of the multiple-ring catheter.

3.4 | Relationship of Gap Width With Biophysical Data

Scatter plots of RCG length versus T_{slow} , T_{nadir} , $i\text{TT}_0$, and $i\text{TT}_{15}$ are shown in Figure 6. The width of RCGs significantly correlated with T_{nadir} ($R = 0.42$; $p = 0.021$) and $i\text{TT}_{15}$ ($R = -0.44$; $p = 0.015$).

3.5 | Follow-Up Data

During a mean follow-up of 21.8 ± 17.1 months, freedom from atrial tachyarrhythmia recurrence was 76.7% of all the patients during the follow-up period. Twenty-one patients underwent recurrence of AF after the 3-month blanking period. Patients in

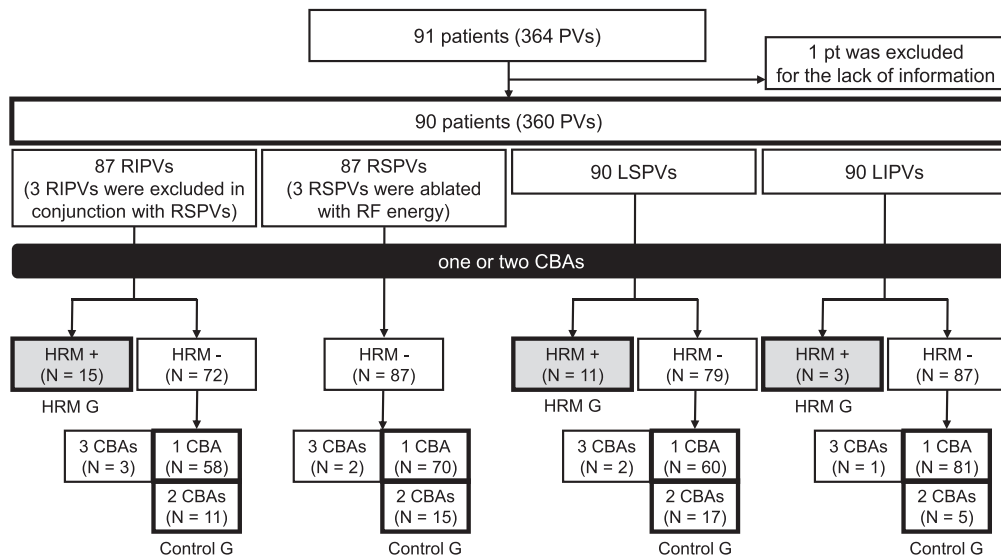


FIGURE 3 | The flowchart of patients. If PV isolation was not accomplished after one or two standard CBAs, HRM was performed to identify RCGs at the discretion of the operator. Twenty-nine PVs in gray boxes were analyzed by HRM, and classified as HRM group. Three hundred seventeen PVs in white boxes were isolated with a total of one or two CBAs and classified as Control group. CBA, cryoballoon application; HRM, high-resolution mapping; LIPV, left inferior pulmonary vein; LSPV, left superior pulmonary vein; pt, patient; PV, pulmonary vein; RCG, resistant conduction gap; RF, radiofrequency; RIPV, right inferior pulmonary vein; RSPV, right superior pulmonary vein.

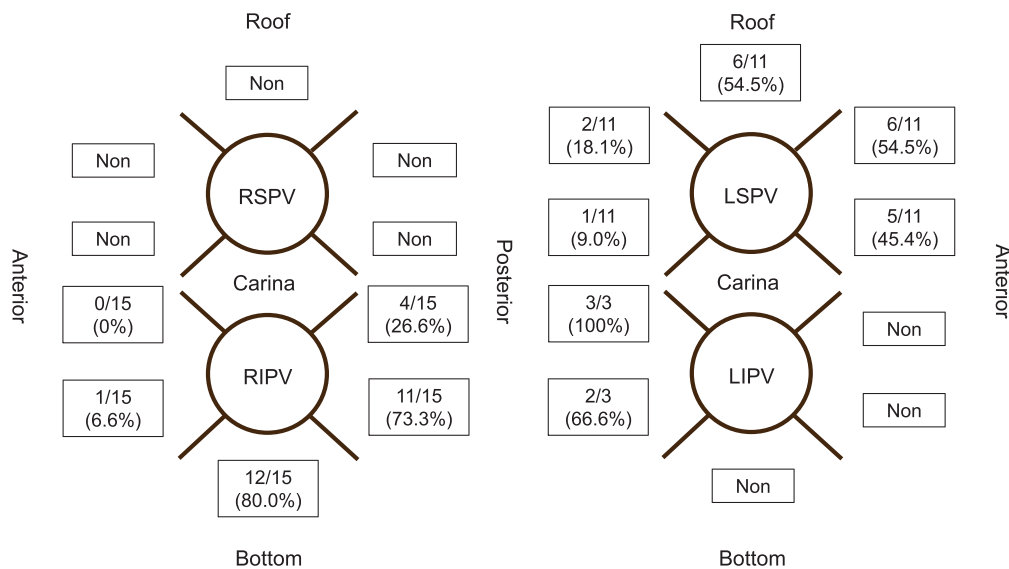


FIGURE 4 | The distribution of RCGs identified by HRM after one or two CBAs. Each RCG was classified into the division of the antrum of each PV. Abbreviations are the same as in Figure 3. [Color figure can be viewed at wileyonlinelibrary.com]

HRM group had a lower recurrence rate of AF than those in Control group (2/29, 6.9% vs. 19/61, 31.1%).

4 | Discussion

To our knowledge, this study represents the first comprehensive and detailed analysis of RCGs during standard PV isolation with CBA for AF. Detailed and accurate RCGs were successfully detected using HRM. The main findings are as follows: (1) The RCGs after standard CBAs were equivalently common in RIPV and LSPV, rarer in the LIPV, and none in RSPV; (2) most of the

RCGs in RIPV spread from the bottom to the posterior wall; (3) most of the RCGs in LSPV spread from the roof to the anterior wall; (4) the width of RCGs was significantly associated with higher T_{nadir} and shorter iTT_{15} ; and (5) most of these identified RCGs were successfully ablated with cryoablation by modifying CB contact based on the location and spread of RCGs.

4.1 | Localization and Spread of RCGs

There are limited data regarding the identification of RCGs after standard CBAs. This is partly because repositioning a CB into

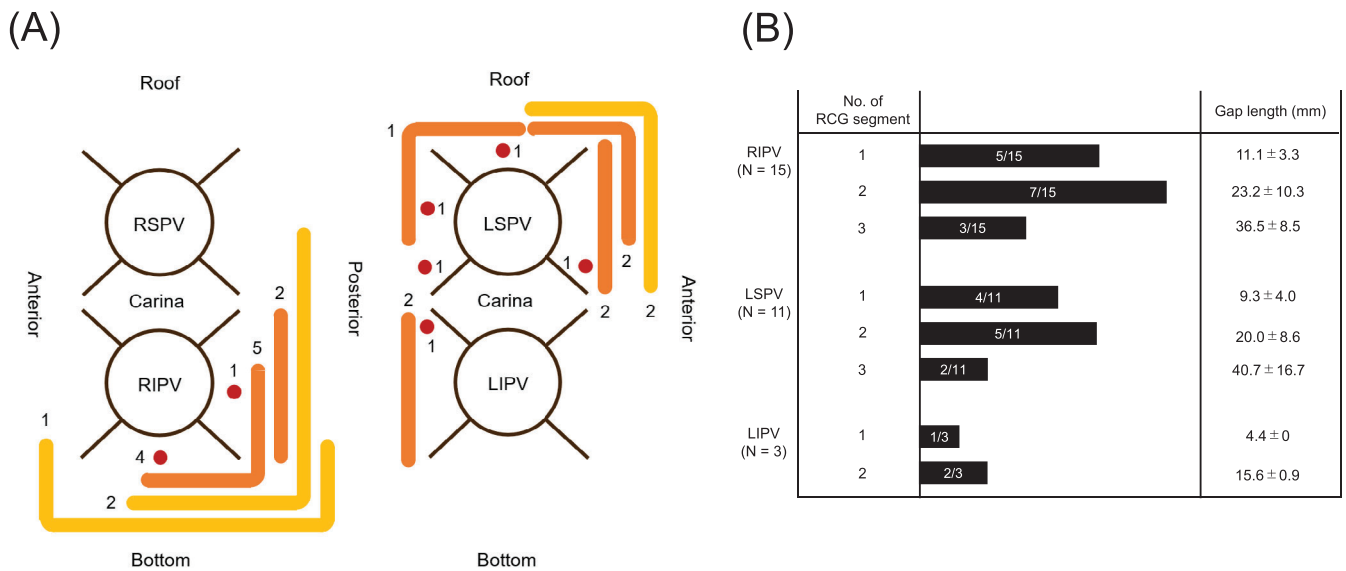


FIGURE 5 | The spread of the RCGs. (A) The distribution of RCGs identified by HRM after one or two CBAs. Red circles, orange bars, and yellow bars indicate 1-segment, 2-segment, and 3-segment gaps, respectively. The adjacent number indicates the number of patients. (B) The number of gap segments and the average total width in each PV. Abbreviations are the same as in Figure 3. [Color figure can be viewed at [wileyonlinelibrary.com](https://onlinelibrary.wiley.com)]

another PV branch rather than identifying and analyzing RCGs has been focused on [7]. The detection rate of the electrical gaps is deeply involved in the resolution of the electrical signals during mapping [8, 9]. Conte et al. demonstrated that atrial re-mapping after CBA using HRM system improves the detection of incomplete ablation areas [10]. Furthermore, Ruiz-Granell et al. reported the detail of gaps after PV isolation using ultra-high-density mapping in patients with pre-CB and pre-RF ablation [11]. They showed that gaps in voltage mapping were wider in pre-CB patients compared with pre-RF patients, and voltage mapping was more effective in gap detection than activation mapping in pre-CB patients, whereas it was vice-versa in pre-RF patients. This finding is consistent with our results that gaps over multiple segments were more recognized compared with a single segment gap after CB ablation (Figure 5).

RIPVs have been reported to be one of the most frequent sites for electrical gaps after CBA. Yasuoka et al. showed that the electrical gaps of RIPV were recognized in 12 out of 30 patients and associated with the angle of insertion into LA and the position from the non-coronary cusp [12]. Matsumoto et al. reported that the rate of incomplete CBA was 20% for RIPVs, followed by 8% in RSPVs, and 4% in LSPVs, and the PV angle was significantly associated with incomplete CBA [13]. Furthermore, Miyazaki et al. demonstrated that the most common reconnection site was the RIPV bottom at the 2nd procedure after CB ablation and more than half of the reconnections were involved in clinical AF recurrence [14]. These results may be explained by the imperfect alignment of the CB ablation system with RIPVs because of a sharp angle and short distance from the atrial septum as the above previous papers reported [12, 13]. As a result, it might cause difficulties in the firm attachment of a CB against the bottom sites. The present study supports this idea with the frequent posteroinferior gaps (80%; 12/15 patients) and the low occlusion grade in RIPV in HRM group (Table 2). In addition, the lower occlusion grade (2.2 ± 0.4) could decrease cooling effects,

presumably associating with frequent multiple segments of RCG in RIPV.

The area from the roof to the anterior wall of LSPV exhibited the second highest rate of RCGs after CBAs whereas the left carina had few RCGs in the present study. Compared to right PVs, left PVs have a higher ovality index [15, 16], which was reported to show an inverse relationship to the degree of PV occlusion [16]. In addition, Kajiyama et al. demonstrated that LSPV required multiple applications for successful isolation, because of a thinner left lateral ridge (<4.7 mm), higher ovality ($>50.5\%$), and longer PV ostium-bifurcation distance (>26.1 mm) [17]. These anatomical parameters could be associated with RCGs in LSPV. It may be difficult to obtain sufficient pushability for oval and sharp ridges. In particular, the roof of LSPV might be hard to cover with the balloon hemisphere even if the balloon and sheath have the correct force and direction. Importantly, 11 patients with LSPV gaps included 7 gaps over multiple segments, which were the most frequently recognized at superior anterior sites of LSPV (63.6%; 7/11 patients). Similarly to RIPV, larger RCGs could also be associated with lower occlusion grade (2.7 ± 0.6), causing decreased cooling effects.

4.2 | Biophysical Parameters (T_{nadir} , iTT_{15})

Conventional biophysical parameters of CB ablation, such as balloon cooling rate, balloon nadir temperature, and balloon thawing time, have been used as effective predictors of durable PV isolation [5, 6, 18]. On the other hand, there are few reports of the parameters to predict optimal lesion formation in clinical practice.

There are several reports of in vivo experiments showing the relationships between CBA and lesion size formation. Takami et al. reported that tissue thermodynamics during CBA depended

TABLE 2 | Comparison of thermodynamic variables between HRM and Control group.

	HRM	Control	<i>p</i> value
RIPV (<i>n</i> = 15) (<i>n</i> = 69)			
No. of CBAs	2.2 ± 0.6	1.4 ± 0.6	<0.001 ^a
Occlusion grade	2.2 ± 0.4	3.4 ± 0.5	<0.001 ^a
T _{slow} (°C)	-30.2 ± 4.5	-34.3 ± 4.6	0.002 ^a
T _{nadir} (°C)	-40.6 ± 6.0	-48.2 ± 6.3	<0.001 ^a
iTT ₀ (s)	6.6 ± 2.2	10.7 ± 4.1	<0.001 ^a
iTT ₁₅ (s)	21.6 ± 9.0	34.3 ± 13.7	0.001 ^a
RSPV (<i>n</i> = 85)			
No. of CBAs	—	1.1 ± 0.3	—
Occlusion grade	—	3.6 ± 0.4	—
T _{slow} (°C)	—	-36.0 ± 4.5	—
T _{nadir} (°C)	—	-51.4 ± 5.9	—
iTT ₀ (s)	—	13.4 ± 4.8	—
iTT ₁₅ (s)	—	41.8 ± 16.5	—
LSPV (<i>n</i> = 11) (<i>n</i> = 77)			
No. of CBAs	2.3 ± 0.5	1.2 ± 0.4	<0.001 ^a
Occlusion grade	2.7 ± 0.6	3.7 ± 0.4	<0.001 ^a
T _{slow} (°C)	-31.1 ± 3.3	-35.0 ± 3.7	0.001 ^a
T _{nadir} (°C)	-42.5 ± 7.2	-48.2 ± 6.4	0.008 ^a
iTT ₀ (s)	8.4 ± 3.9	11.1 ± 3.3	0.018 ^a
iTT ₁₅ (s)	27.3 ± 15.1	39.8 ± 14.6	0.018 ^a
LIPV (<i>n</i> = 3) (<i>n</i> = 86)			
No. of CBAs	3.0 ± 0	1.1 ± 0.2	<0.001 ^a
Occlusion grade	3.3 ± 0.5	3.8 ± 0.4	0.05
T _{slow} (°C)	-32.3 ± 4.7	-33.5 ± 3.6	0.58
T _{nadir} (°C)	-41.6 ± 3.0	-44.9 ± 5.1	0.27
iTT ₀ (s)	7.0 ± 2.6	9.3 ± 3.4	0.25
iTT ₁₅ (s)	14.6 ± 6.0	33.5 ± 13.4	0.018 ^a

Note: Values are presented as mean ± SD.

Abbreviations: CBA, cryoballoon application; HRM, high-resolution mapping; iTT₀, interval thaw time at 0°C; iTT₁₅, interval thaw time at 15°C; LIPV, left inferior pulmonary vein; LSPV, left superior pulmonary vein; PV, pulmonary vein; RIPV, right inferior pulmonary vein; RSPV, right superior pulmonary vein; SD, standard deviation.

^aSignificant *p* value.

on the distance from a balloon and peri-balloon blood flow leak in dog heart experiments. In that study, the warming effect of leak flow was pointed out to be more important because the tissue temperature did not decrease despite the close placement of a CB in the presence of the leak flow, and the blood flow leak location was concordant with chronic reconnection [19]. Wood et al. also reported the impact of superfusate flow on lesion formation using catheter-based CBA in porcine left ventricular myocardial tissues. The experiments showed that the superfusate flow warmed the tissue temperatures and reduced lesion volume when compared with no flow conditions. In addition, they demonstrated catheter electrode temperature predicted lesion size or tissue temperatures

[20]. Furthermore, it has been reported that the CB nadir temperature additionally decreases by the pull-down technique for leak flow sites [21, 22]. The above findings demonstrate that blood flow leak is one of the important factors for CB lesion formation, and the electrode temperature of CB is likely to become the surrogate marker of leak flow which is difficult to analyze quantitatively. This idea is consistent with the findings in the present study that T_{nadir} and iTT₁₅ correlated with the width of RCG presumably reflecting the regional leak flow.

4.3 | Clinical Implications

There are some challenging cases in conventional PV isolation even after multiple CBAs. If PV isolation was not completed, the morphology of PV or the positional relation between CB and targeted PV should be estimated based on the location of the peri-balloon contrast leak to plan the next ablation site, balloon angle, or target branches for placement of the Achieve catheter. However, these assessments reviewing the PV venogram of the current ablation would not be necessarily sufficient to assess balloon contact. The knowledge of the location and width of RCGs could indicate the target to be aimed at, leading to successful PV isolation in challenging cases. The present study revealed the frequent RCG sites in challenging cases of CB ablation where PV isolation failed with 1 or 2 CBAs: the posterior wall to the bottom of RIPV and the anterior wall to the roof of LSPV. In addition, we suggested that balloon biophysical parameters, such as T_{nadir} and iTT₁₅, could become surrogate parameters indicating the size of RCGs. These results could help the operator visualize a CB contacting PV ostium, enabling him or her to perform a more effective CBA to RCGs.

4.4 | Limitations

There are several limitations to be stated. First, the results represent the experience of a single center and might have been influenced by the small size of the study population. Second, this study represents a retrospective analysis examining an association between several procedural and biophysical variables and PV conduction gaps at the repeat procedure. As such, it does not provide prospective validation with respect to any of the study findings. Thus, caution should be paid when the present findings are discussed with the general population. Third, there is a possibility that certain areas of the RCG, especially carina, were not the true gaps of cryoablation because of its definition in the present study. In addition, we were unable to demonstrate whether the identification of RCGs with HRM improves the durability of the PV isolation. On the other hand, the carina area could be involved in the recurrence in CBA as well as RF [23, 24]. Therefore, the data of the RCG in the present study might give useful information on the weakness of CBA compared with extensive encircling PV isolation. Fourth, we were unable to examine the association of the variation of LA anatomy with the location and size of RCG. Although Hayashi et al. reviewed the anatomical difficulty for CB ablation, further studies are needed to elucidate how a CB contacts individual PV ostium with various anatomy [4]. Fifth, insufficient CBAs shorter than 120 s, which were not analyzed in this study, could have had some effect on the results.

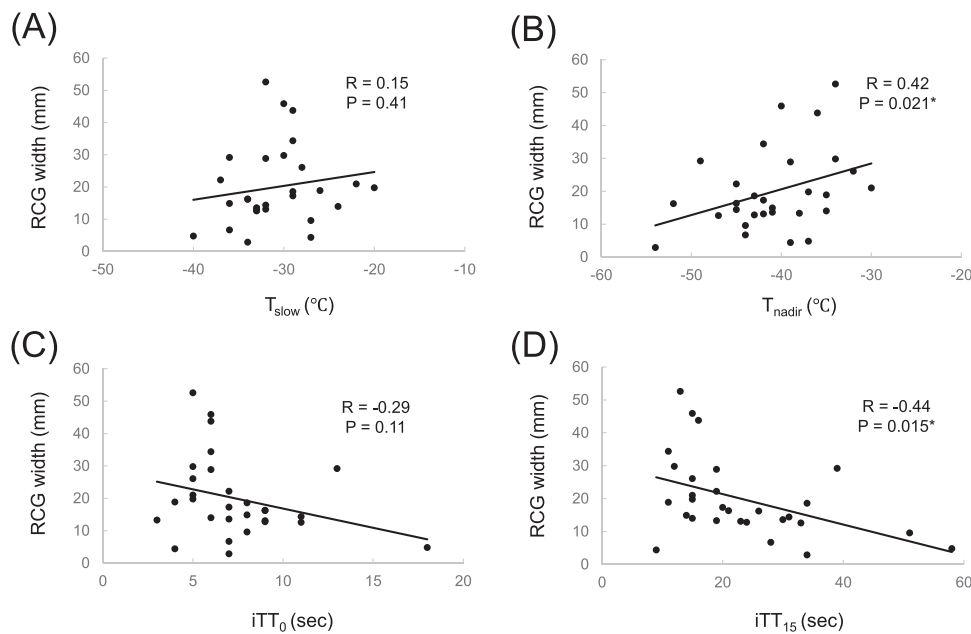


FIGURE 6 | The Scatter plot of RCG width versus (A) T_{slow} , (B) T_{nadir} , (C) iTT_0 , and (D) iTT_{15} . Trend lines, Spearman's rho, and corresponding p values are shown. Abbreviations are the same as in Figure 2.

5 | Conclusion

After standard CBAs, most RCGs were demonstrated to spread from the bottom to the posterior wall of RIPV and from the roof to the anterior wall of LSPV. The width of the RCGs was found to be correlated with parameters of balloon temperature, such as T_{nadir} and iTT_{15} .

Acknowledgments

The authors are deeply grateful to the medical staffs at International University Health and Welfare Hospital.

Disclosure

The authors have nothing to report.

Conflicts of Interest

The authors declare no conflicts of interest.

Data Availability Statement

The majority of data associated with this study is provided in text and figures. Additional data will be made available upon request.

References

1. C. T. January, L. S. Wann, J. S. Alpert, et al., "2014 AHA/ACC/HRS Guideline for the Management of Patients With Atrial Fibrillation: Executive Summary: A Report of the American College of Cardiology/American Heart Association Task Force on Practice Guidelines and the Heart Rhythm Society," *Circulation* 130 (2014): 2071–2104.
2. M. Haïssaguerre, P. Jaïs, D. C. Shah, et al., "Spontaneous Initiation of Atrial Fibrillation by Ectopic Beats Originating in the Pulmonary Veins," *New England Journal of Medicine* 339 (1998): 659–666.
3. K. Kuck, J. Brugada, A. Fürnkranz, et al., "Cryoballoon or Radiofrequency Ablation for Atrial Fibrillation," *New England Journal of Medicine* 374 (2016): 2235–2245.
4. T. Hayashi, M. Murakami, S. Saito, and K. Iwasaki, "Characteristics of Anatomical Difficulty for Cryoballoon Ablation: Insights From CT," *Open Heart* 9 (2022): e001724.
5. N. Deubner, H. Greiss, E. Akkaya, et al., "The Slope of the Initial Temperature Drop Predicts Acute Pulmonary Vein Isolation Using the Second-Generation Cryoballoon," *Europace* 19 (2017): 1470–1477.
6. A. Aryana, G. Mugnai, S. M. Singh, et al., "Procedural and Biophysical Indicators of Durable Pulmonary Vein Isolation During Cryoballoon Ablation of Atrial Fibrillation," *Heart Rhythm* 13 (2016): 424–432.
7. G. B. Chierchia, G. Mugnai, E. Ströker, et al., "Incidence of Real-Time Recordings of Pulmonary Vein Potentials Using the Third-Generation Short-Tip Cryoballoon," *Europace* 18 (2016): 1158–1163.
8. E. Anter, C. M. Tschabrunn, and M. E. Josephson, "High-Resolution Mapping of Scar-Related Atrial Arrhythmias Using Smaller Electrodes With Closer Interelectrode Spacing," *Circulation: Arrhythmia and Electrophysiology* 8 (2015): 537–545.
9. C. Y. Lin, A. L. D. Te, Y. J. Lin, et al., "High-Resolution Mapping of Pulmonary Vein Potentials Improved the Successful Pulmonary Vein Isolation Using Small Electrodes and Inter-Electrode Spacing Catheter," *International Journal of Cardiology* 272 (2018): 90–96.
10. G. Conte, K. Soejima, C. de Asmundis, et al., "Value of High-Resolution Mapping in Optimizing Cryoballoon Ablation of Atrial Fibrillation," *International Journal of Cardiology* 270 (2018): 136–142.
11. R. Ruiz-Granell, G. Ballesteros, D. Andreu, et al., "Differences in Scar Lesion Formation Between Radiofrequency and Cryoballoon in Atrial Fibrillation Ablation: A Comparison Study Using Ultra-High-Density Mapping," *Europace* 21 (2019): 250–258.
12. R. Yasuoka, T. Kurita, Y. Kotake, et al., "Particular Morphology of Inferior Pulmonary Veins and Difficulty of Cryoballoon Ablation in Patients With Paroxysmal Atrial Fibrillation," *Circulation Journal* 81 (2017): 668–674.
13. Y. Matsumoto, Y. Muraoka, Y. Funama, et al., "Analysis of the Anatomical Features of Pulmonary Veins on Pre-Procedural Cardiac CT Images Resulting in Incomplete Cryoballoon Ablation for Atrial

- Fibrillation," *Journal of Cardiovascular Computed Tomography* 13 (2019): 118–127.
14. S. Miyazaki, H. Taniguchi, H. Hachiya, et al., "Clinical Recurrence and Electrical Pulmonary Vein Reconnections After Second-Generation Cryoballoon Ablation," *Heart Rhythm* 13 (2016): 1852–1857.
15. M. Schmidt, U. Dorwarth, F. Straube, et al., "Cryoballoon in AF Ablation: Impact of PV Ovality on AF Recurrence," *International Journal of Cardiology* 167 (2013): 114–120.
16. A. Sorgente, G. B. Chierchia, C. de Asmundis, et al., "Pulmonary Vein Ostium Shape and Orientation as Possible Predictors of Occlusion in Patients With Drug-Refractory Paroxysmal Atrial Fibrillation Undergoing Cryoballoon Ablation," *Europace* 13 (2011): 205–212.
17. T. Kajiyama, S. Miyazaki, J. Matsuda, et al., "Anatomic Parameters Predicting Procedural Difficulty and Balloon Temperature Predicting Successful Applications in Individual Pulmonary Veins during 28-mm Second-Generation Cryoballoon Ablation," *JACC Clinical Electrophysiology* 3 (2017): 580–588.
18. J. Ghosh, A. Martin, A. C. Keech, et al., "Balloon Warming Time Is the Strongest Predictor of Late Pulmonary Vein Electrical Reconnection Following Cryoballoon Ablation for Atrial Fibrillation," *Heart Rhythm* 10 (2013): 1311–1317.
19. M. Takami, J. Misiri, H. I. Lehmann, et al., "Spatial and Time-Course Thermodynamics During Pulmonary Vein Isolation Using the Second-Generation Cryoballoon in a Canine in Vivo Model," *Circulation: Arrhythmia and Electrophysiology* 8 (2015): 186–192.
20. M. A. Wood, B. Parvez, A. L. Ellenbogen, et al., "Determinants of Lesion Sizes and Tissue Temperatures During Catheter Cryoablation," *Pacing and Clinical Electrophysiology* 30 (2007): 644–654.
21. K. R. Chun, B. Schmidt, A. Metzner, et al., "The 'Single Big Cryoballoon' Technique for Acute Pulmonary Vein Isolation in Patients With Paroxysmal Atrial Fibrillation: A Prospective Observational Single Centre Study," *European Heart Journal* 30 (2009): 699–709.
22. H. Ahmed, P. Neuzil, J. Skoda, et al., "The Permanency of Pulmonary Vein Isolation Using a Balloon Cryoablation Catheter," *Journal of Cardiovascular Electrophysiology* 21 (2010): 731–737.
23. T. Nanbu, A. Yotsukura, F. Sano, et al., "A Relation Between Ablation Area and Outcome of Ablation Using 28-mm Cryoballoon Ablation: Importance of carina Region," *Journal of Cardiovascular Electrophysiology* 29 (2018): 1221–1229.
24. R. Proietti, P. Santangeli, L. Biase, et al., "Comparative Effectiveness of Wide Antral Versus Ostial Pulmonary Vein Isolation: A Systematic Review and Meta-Analysis," *Circulation: Arrhythmia and Electrophysiology* 7 (2014): 39–45.